Preparation of energy storage material derived from a used cigarette filter for a supercapacitor electrode

2014 Nanotechnology 25 345601

(http://iopscience.iop.org/0957-4484/25/34/345601)

IOP Publishing Nanotechnology
Nanotechnology **25** (2014) 345601 (8pp) doi:10.1088/0957-4484/25/34/345601

Preparation of energy storage material derived from a used cigarette filter for a supercapacitor electrode

Minzae Lee[1], Gil-Pyo Kim[1], Hyeon Don Song, Soomin Park and Jongheop Yi

World Class University (WCU) program of Chemical Convergence for Energy & Environment, School of Chemical and Biological Engineering, College of Engineering, Seoul National University, Shillim-dong, Kwanak-gu, Seoul 151-742, Korea

E-mail: jyi@snu.ac.kr

Received 24 April 2014, revised 2 June 2014
Accepted for publication 19 June 2014
Published 5 August 2014

Abstract

We report on a one-step method for preparing nitrogen doped (N-doped) meso-/microporous hybrid carbon material (NCF) via the heat treatment of used cigarette filters under a nitrogen-containing atmosphere. The used cigarette filter, which is mostly composed of cellulose acetate fibers, can be transformed into a porous carbon material that contains both the mesopores and micropores spontaneously. The unique self-developed pore structure allowed a favorable pathway for electrolyte permeation and contact probability, resulting in the extended rate capability for the supercapacitor. The NCF exhibited a better rate capability and higher specific capacitance (153.8 F g^{-1}) compared to that of conventional activated carbon (125.0 F g^{-1}) at 1 A g^{-1}. These findings indicate that the synergistic combination of well-developed meso-/micropores, an enlarged surface area and pseudocapacitive behavior leads to the desired supercapacitive performance. The prepared carbon material is capable of reproducing its electrochemical performance during the 6000 cycles required for charge and discharge measurements.

S Online supplementary data available from stacks.iop.org/NANO/25/345601/mmedia

Keywords: cigarette filter, nonbiodegradable biomass, recycle, carbonization, supercapacitor

(Some figures may appear in colour only in the online journal)

1. Introduction

Supercapacitors are attracting attention as an energy storage system (ESS) due to their high power density, short charging time and long cycle life [1–3]. They are of considerable interest in various applications, such as electrical vehicles, micro sensors and portable electronics [4–7]. For such applications, it is important to develop an advanced generation of supercapacitors that have the capability to supply high levels of power and energy [8]. Therefore, the selection of the proper electrode material is one of the most important parameters in improving the performance of supercapacitors.

Carbon is one of the promising materials considered for use in supercapacitors due to its low cost, high porosity, electronic conductivity and stability [8]. For a high-performance supercapacitor, electrode materials with a high surface area and proper pore size distribution are essential in utilizing a large amount of electrolyte ions with quick transfer mobility at the surface of the electrode material [9]. It has been reported that the mesopores (2–50 nm) can provide desirable pathways for the movement of electrolyte ions [10], while the micropores (<2 nm) further increase the surface area in order to enhance the electrical double-layer capacitance (EDLC) [11]. In addition, chemical doping with heteroatoms, especially nitrogen, can largely enhance the capacitance of a carbon material by supplying pseudocapacitive interactions

[1] Co-first authors, equal contributions.

[12]. Therefore, the development of carbon electrode material with a well-developed meso-/micropore structure and with pseudocapacitive assistance can largely improve supercapacitive performance. Although various attempts have been made to prepare nitrogen-doped carbon materials with a porous structure, most methods involve the use of commercial activated carbon sources and include post-doping routes, which include high energy consumption and multi-step processes [13].

Used cigarette filters are composed largely of cellulose acetate. They are disposable, non-biodegradable, toxic and are a threat to the environment after usage. However, it has been reported that cellulose acetate can be directly utilized in the production of carbon materials containing a meso-/micropore structure by only a carbonization process [14]. That is, used cigarette filters could be used as a proper carbon source for supercapacitors. Importantly, carbonizing used cigarette filters in a nitrogen-containing atmosphere could provide the nitrogen doping on the carbon structure with the formation of such unique pore structures in a one-step process.

In the findings reported herein, the nitrogen-doped porous carbon material derived from a used cigarette filter was employed as an active material for the supercapacitor. Taking advantage of the above-mentioned properties, our concept efficiently supports the combined virtues associated with recycling severe solid waste and developing a cost-competitive supercapacitor material. The present work focuses on (1) recycling used cigarette filters as a carbon source for use in a supercapacitor, (2) characterizing the pore structure and the nitrogen-doping states of the prepared material and (3) studying the effect of physicochemical characteristics on the electrochemical properties of the product. To the best of our knowledge, a study of the feasibility of preparing porous carbon materials derived from used cigarette filters for use in supercapacitors has not been reported.

2. Experimental

2.1. Preparation of active materials for the supercapacitor

Used cigarette filters from Marlboro Light Gold (Philip Morris Int.), Bohem Cigar Mojito and The One Orange (Korea Tobacco & Ginseng Corp.) were collected. Since activated carbon particles coexist in half of the total part of the filters for Marlboro Light Gold and The One Orange as an adsorbent, we only utilized the other half of the filters in order to exclude the effect of pre-contained activated carbon for the precise characterization of the electrode material. CF and NCF were fabricated from the filters under an atmosphere of Ar and NH_3 at 900 °C for 2 hrs, respectively. The heating rate was controlled at 5 °C min^{-1}. Identical masses of filters from each brand were used in preparing these materials. No pretreatment on the used cigarette filters was conducted before the carbonization process in order to minimize the fabrication procedure and the cost for the production of the supercapacitor electrode. The specific mass ratio ($1/8 \sim 1/10$) of both the CF and the NCF for the original mass of cigarette filters were prepared. MSP-20 (Kansai Coke) was used as an activated carbon (AC). Bare TiO_2 was synthesized by a gel-hydrothermal method and N-doped TiO_2 was synthesized by a post treatment of bare TiO_2 under the same conditions as for the NCF [15].

2.2. Material characterization

The surface morphology of the CF was characterized using a high-resolution transmission electron microscopy (HR-TEM, JEOL, JEM-3010) and scanning electron microscopy (SEM, Carl Zeiss, SUPRA 55VP). X-ray photoelectron spectroscopy (XPS, Kratos, AXIS-HSI) was used to investigate the elemental species and the binding states of the prepared samples. An x-ray diffractometer (XRD, Rigaku, D/max-2500/PC) using Cu Kα radiation (wavelength = 0.154 nm) as an incident beam at 50 kV and 100 mA was utilized to confirm the crystalline and elemental structure of the composite. N_2 adsorption-desorption isotherms were measured with a Micromeritics ASAP 2010 instrument. The Brunauer–Emmett–Teller (BET) method was utilized to calculate the specific surface area. The pore volume and pore size distributions were derived from the desorption branches of the isotherms using the Barrett–Joyner–Halenda (BJH) method. The mass ratio of the impurities was calculated based on the data obtained from a thermogravimetric analyzer (TGA, Versa Therm, Thermo Scientific) with a heating rate of 10 °C min^{-1} in air. The amount of nitrogen in the NCF was determined using a C, H, N, S analyzer (CHNS 932, LECO). The elemental analysis of the bulk phase was performed by inductively coupled plasma with atomic emission spectrometry (ICP-AES, Shimadzu, JP/ICPS-7500).

2.3. Preparation of electrodes

A standard three-electrode system was used with a KCl saturated Ag/AgCl as a reference electrode and a platinum counter electrode. The active materials (NCF, CF and AC) were mixed with polytetrafluoroethylene (PTFE, Aldrich) as a binder and as a carbon additive (ketjenblack ECP-600JD, KB) in a mass ratio of 8:1:1. The mixture was coated onto 1 cm × 1 cm nickel foam as the current collector. After coating the electrode materials, the working electrode was pressed and dried in a vacuum at 120 °C for 12 h.

2.4. Electrochemical measurements

The analyses were conducted in 6.0 M KOH aqueous electrolyte at room temperature. The Cyclic voltammograms (CVs) and galvanostatic charge-discharge measurement were performed on an electrochemical workstation (Iviumstat electrochemical analyzer, Ivium Technology). The CVs were recorded in the potential range of −0.8 to 0 V by varying the scan rate from 5 to 100 mV s^{-1}. Galvanostatic charge-discharge testing was performed by varying the current density from 1.0 to 10 A g^{-1} with a potential window of −0.8 to 0 V. The electrochemical impedance spectroscopy (EIS) of the electrode was performed on an electrochemical workstation (WonA tech, ZIVE SP2). The frequency of the EIS ranged

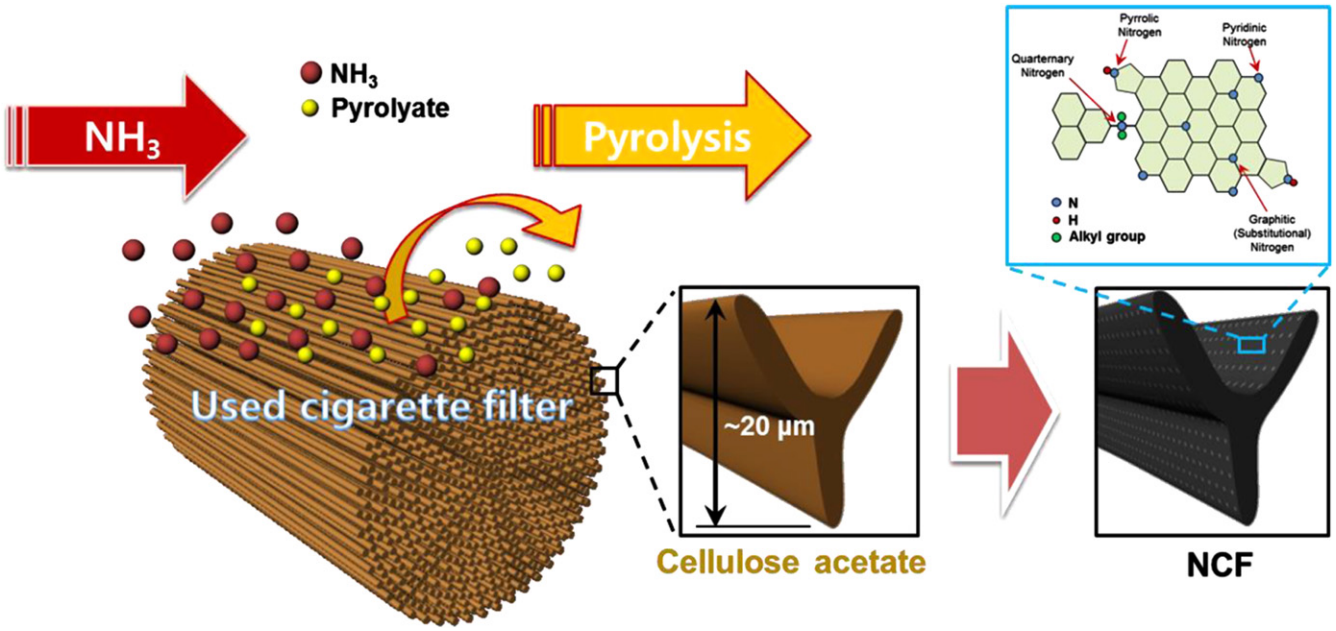

Scheme 1. Schematic representation of the fabrication process used for preparing the NCF by pyrolysis of a used cigarette filter.

from 20 mHz to 200 kHz at an applied potential of −0.4 V and an AC amplitude of 10 mV.

2.5. Calculation

The specific capacitance ($F\,g^{-1}$) was calculated from the discharge curves of the galvanostatic charge-discharge results by the following equation [16].

$$C = \frac{I\Delta t}{m\Delta V} \quad (1)$$

where I is the constant discharge current, Δt is the discharging time, ΔV is the discharging voltage and m is the mass of the active material. ΔV is the voltage, excluding the IR drop occurring at the beginning of the discharge.

3. Results and discussion

Scheme 1 illustrates the synthetic procedure used to prepare an NCF by a pyrolysis. Typically, various polymers can be easily transformed into a carbon material in the presence of Ar and NH_3, leading to the formation of a unique pore structure [17, 18]. Figure 1(a) shows the features of the NCF powder and the used cigarette filters. Figure 1(b) reveals the morphology of the cellulose acetate fibers of a used cigarette filter. Figures 1(c) and (d) show SEM and TEM images of the NCF flakes, respectively. In figure 1(d), the pores (white dots) are elucidated within the material after the carbonization process.

Crystalline properties of the NCF, CF and N-doped TiO_2 were investigated for basal characterization. The broad x-ray structures of the NCF and the carbons obtained by annealing with Ar from non-smoked cigarette filters (PCF, all brands mixed) and from each brand are indicative of amorphous carbon, as shown in figure 2. The two broad peaks positioned at $20\sim25$ and $40\sim45$ of 2θ for prepared carbon samples indicate the incomplete graphitization by pyrolysis at a relatively low temperature of 900 °C [19]. Interestingly, Peaks for anatase TiO_2 were detected after the carbonization process for all of the as-prepared materials. This result reveals that Ti species do not originate from the cigarette smoke or a specific cigarette filter. TiO_2 is a commonly used additive material during the fabrication of a cigarette filter in order to induce the photo-degradation of the cellulose acetate in ambient surroundings and to whiten the color of the filters [20]. N-doped TiO_2 and TiN were observed in the NCF. TiN begins to be produced from bare TiO_2 while annealing with ammonia at a temperature of over 680 °C with a formation of N-doped TiO_2 [15].

Elements that are known to be present in the cigarette smoke, such as Cd, Cr and As, were not detected by an inductively coupled plasma analysis (ICP). This may be due to their low concentrations (<1 ppm) [21]. The mass ratios of the impurities compared to the total mass of the CF and the NCF were ~3.6 wt%, which is obtained by TGA analysis, as shown in figure 3; and the amount of nitrogen contents in the NCF was 7 wt%, which was proved by CHNS analysis.

The porosity properties of the resultant carbon materials by N_2 sorption isotherms are summarized in figure 4(a) and in table 1. It can be seen that the porosity characteristics of the NCF and the CF are considerably different from the AC. The AC showed the isotherm for type-I, which is a general form of microporous structure. However, the isotherms of the NCF and the CF exhibited the type-IV with a slight increase of the slope at higher relative pressures compared to that of the AC. This is typically caused by capillary condensation-evaporation in mesopores. A hysteresis loop constructed from P $P_0^{-1} = 0.45$ to 0.8 for the NCF and the CF are caused by the coexistence of both meso- and micropores. Furthermore, it

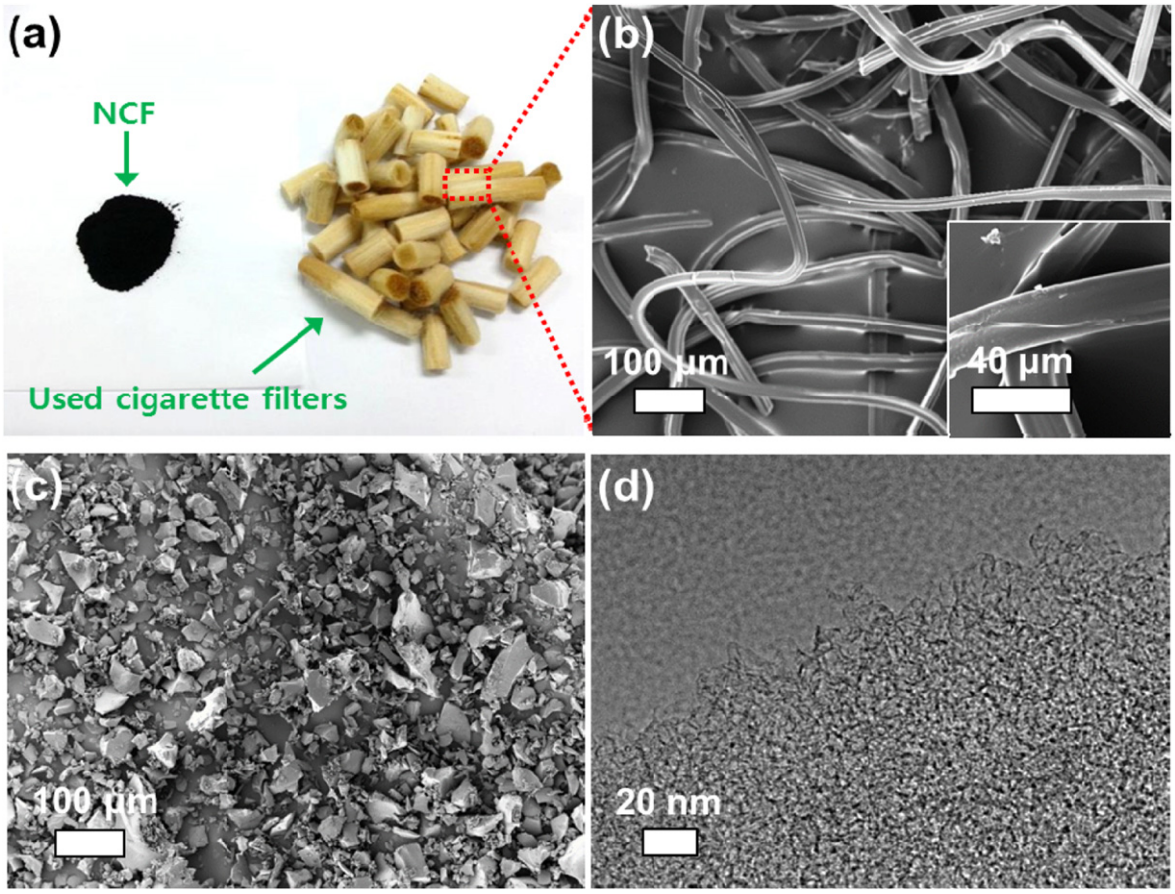

Figure 1. (a) Photograph of the NCF powder and the used cigarette filters. SEM image of the (b) used cigarette filter and the (c) NCF, respectively. (d) HR-TEM image of the NCF.

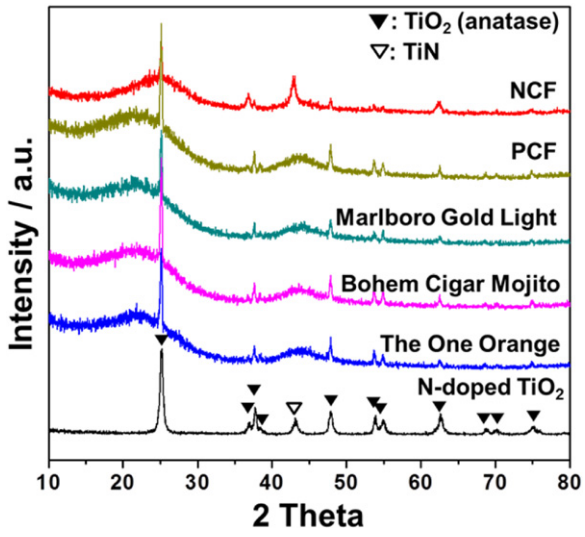

Figure 2. XRD patterns of the NCF, the N-doped TiO_2 and the carbons obtained by annealing with Ar from non-smoked cigarette filters (PCF, all brands mixed) and from a used cigarette filter (each brand).

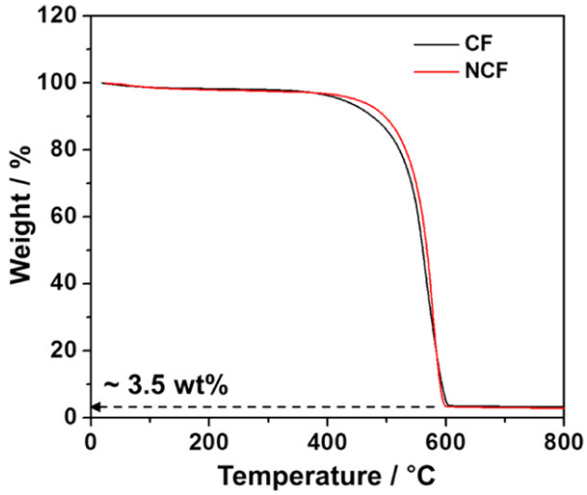

Figure 3. TGA results of the NCF and the CF.

should be noted that the mesopores (3.3 ~ 4.2 nm) for the NCF and the CF can be beneficial to the easy approach of the electrolyte ions into the pores located deep inside the surface of a particle, as shown in figure 4(b), which are also important for fast electrolyte ion transfer. On the other hand, the majority of the pores for the AC were smaller than ~2 nm, indicating that the percolation of the electrolyte ions into the pores of the AC electrode could be restricted. The specific surface area of the NCF was larger than that of the CF, as shown in table 1, because the doped nitrogen plays a role in the carbon gasification at over 700 °C, which leads to the formation of additional pores [22]. The mesoporous ratios for

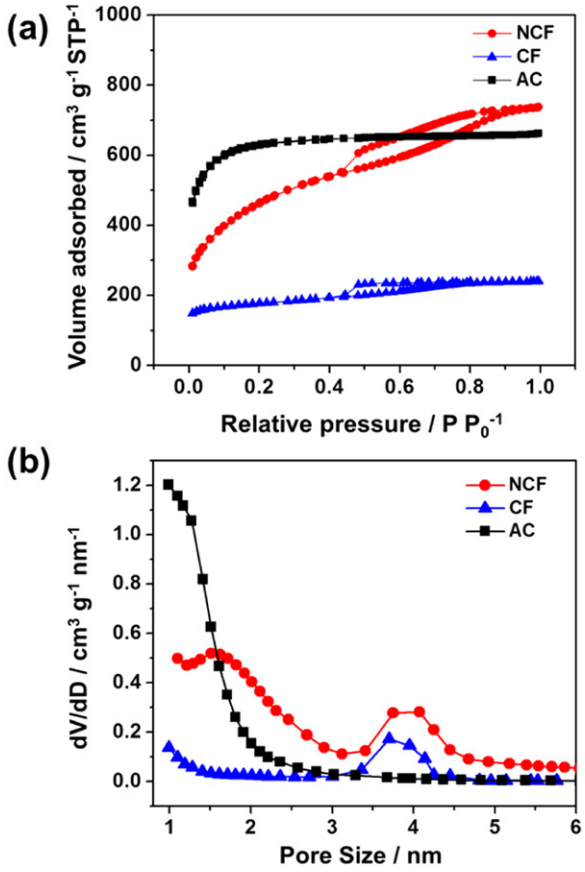

Figure 4. (a) N_2 adsorption-desorption isotherms. (b) BJH pore size distributions of the NCF, the CF and the AC.

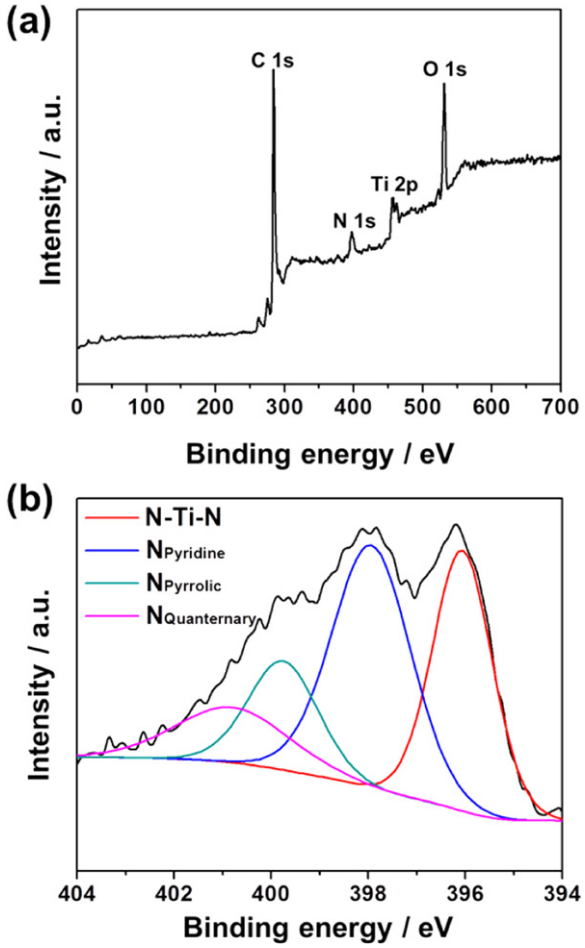

Figure 5. XPS spectra of the (a) expanded region and the (b) N1s region of the NCF with deconvoluted spectra.

CF, NCF and AC in the total surface area were estimated to be 31.06%, 44.68% and 0%, respectively. The binding energy of the chemically bonded nitrogen atoms within the NCF were 396.1 eV, 397.9 eV, 399.8 eV and 400.8 eV, which are assigned to N-Ti-N bonding from Ti species, pyridine, pyrrolic or pyridone, and quaternary species, respectively, as shown in figure 5 [23, 24]. The highest amount of pyridinic nitrogen (39.5 atom%) was observed in the NCF, which can provide the pseudocapacitive interaction between the electrolyte ions in an alkaline electrolyte [12].

The obtained NCF was applied as electrode materials for the supercapacitor. The electrochemical properties of the prepared NCF were evaluated via galvanostatic charge-discharge measurements (figure 6(a)) and cyclic voltammograms (CVs) (figure 6(b)). These analyses were performed in a potential window of −0.8 to 0 V in 6.0 M KOH aqueous solution with a three electrode system.

The charge and discharge behaviors of the NCF electrode were examined at current densities in the range from 1 to 10 A g^{-1}. The charge-discharge curves of the NCF show a symmetrical triangle shape with a small internal resistance (IR) drop at a current density of 1 A g^{-1}, indicating a high degree of symmetry in the charge and the discharge [25]. The presence of the IR drop at the initial point of the discharging curve at 1 A g^{-1} corresponds to the equivalent series resistance (ESR) [26]. The CVs for the NCF electrode were evaluated at scan rates ranging from 5 to 100 mV s^{-1}. The CVs for the NCF electrode have an asymmetrical quasi-rectangular shape, which is due to the charge resistance of the electrodes in the potential range of −0.8 V to 0 V. Despite the asymmetry of the CVs of the NCF, the shapes of the CVs were well retained, in accordance with the increase of the scan rates, which indicate that the NCF retains its substantial capacitive properties, even at a high scan rate of 100 mV s^{-1}. If the ions from the electrolyte are able to easily approach the electrochemically active surface of the electrode, the charge-discharge capabilities become faster with the increase of the scan rate, which indicates the favorable reversibility of a supercapacitor [23].

The supercapacitive performance of the NCF was further compared with the CF and the AC, as shown in figure 6(c). The results of the electrochemical performance for the CF and the AC are shown in figure S1. The discharging time of the NCF was obviously longer than those of the other samples, as shown in figure 6(c), which reveals the highest specific capacitance. The specific capacitances of NCF, CF and AC were compared, as shown in figure 6(d). The decrease in specific capacitances with increasing current density for all of the electrode materials is due to the increase in the charge resistance of the material [27]. The lower specific capacitance

Table 1. BET surface area and porosity characteristics of the NCF, the CF and the AC.

Active Materials	S_{BET} ($m^2\ g^{-1}$)	$S_{micropore}$ ($m^2\ g^{-1}$)	$S_{mesopore}$ ($m^2\ g^{-1}$)	$V_{total\ pore}$ ($cm^3\ g^{-1}$)	$V_{micropore}$ ($cm^3\ g^{-1}$)	$V_{mesopore}$ ($cm^3\ g^{-1}$)	$D_{average}$ (nm)
NCF	1634	904	730	1.2571	0.3609	0.8962	2.38
CF	573	395	178	0.2221	0.1951	0.0270	2.49
AC	1989	1989	—	0.7967	0.7967	—	1.36

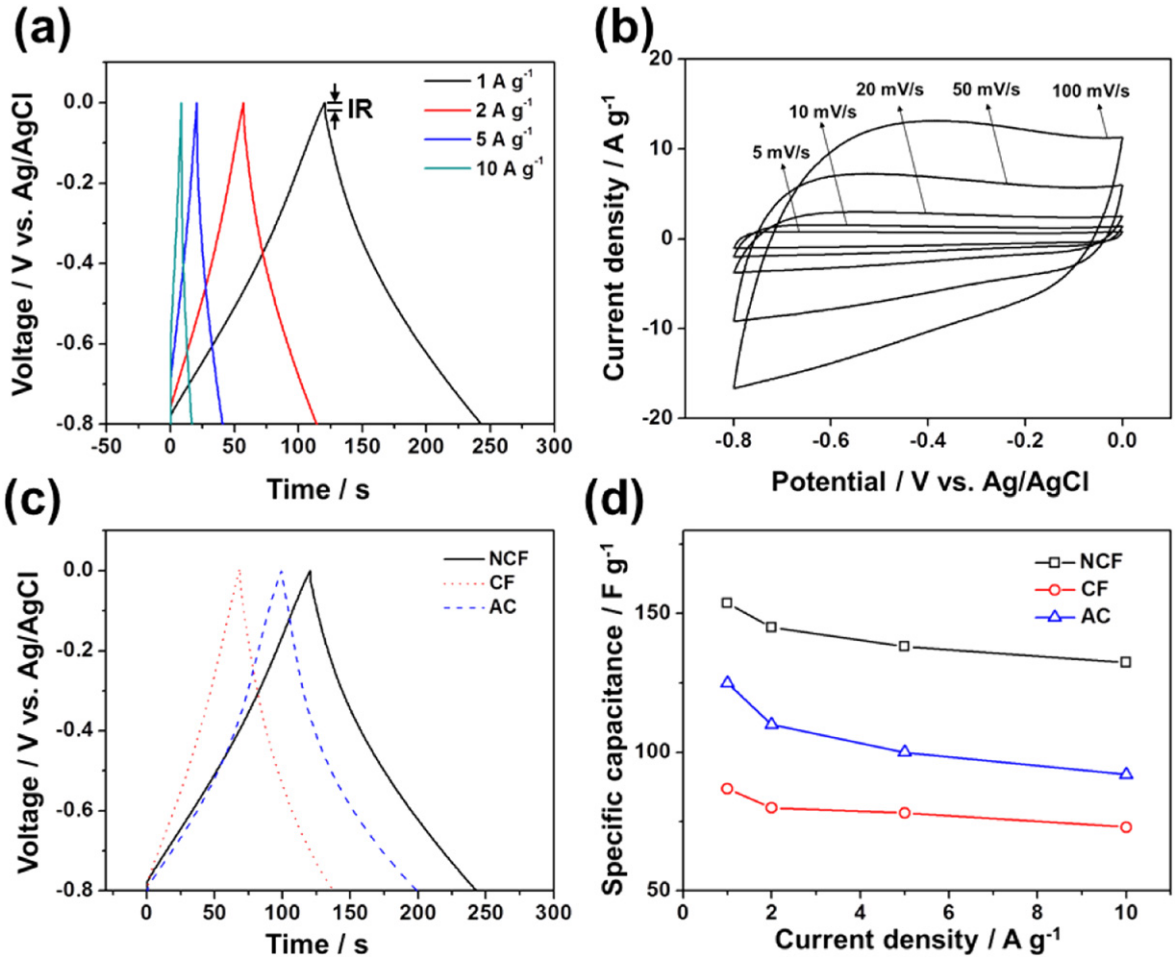

Figure 6. (a) Charge-discharge curves of the NCF electrode at different current densities. (b) CVs of the NCF electrode from 5 to 100 mV s^{-1}. (c) Comparison of charge-discharge curves of the NCF, the CF and the AC at 1 A g^{-1}. (d) Calculated specific capacitances of the NCF, the CF and the AC from the galvanostatic discharge curves at different current densities.

of the CF compared to that of the AC is due to the fact that the lower surface area. The rate capabilities of the NCF and the CF were better than that of the AC by means of the changes in specific capacitances. This is due to the presence of higher mesoporous ratios compared to that of the AC, which serve as a favorable pathway for electrolyte ion movement. The NCF electrode has specific capacitances of 153.8, 145.0, 138.2 and 132.4 F g^{-1} at current densities of 1, 2, 5 and 10 A g^{-1}, which are higher than those of CF and AC electrodes. Importantly, the specific capacitance of the NCF at 5 A g^{-1} (138.2 F g^{-1})

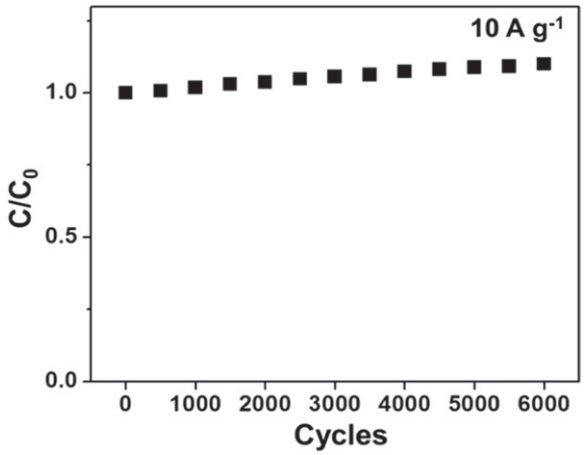

Figure 7. Cycle life of the NCF electrode by a charge-discharge measurement during 6000 cycles at 10 A g^{-1}.

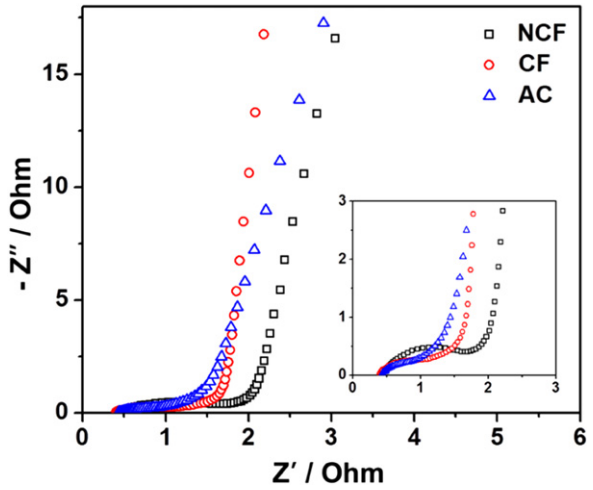

Figure 8. Nyquist impedance plots of the NCF, the CF and the AC at an applied potential of −0.4 V, an AC amplitude of 10 mV and frequencies from 20 mHz to 200 kHz.

exceeds the values for the CF and the AC at a lower current density (1 A g^{-1}), 86.9 F g^{-1} and 125.0 F g^{-1}, respectively. This higher current density indicates that a higher energy for quick action is available, which is essential for ideal capacitive behavior. This may be ascribed to the synergistic contribution of the enlarged high surface area, the proper pore structure and the superior surface functionalities of the NCF, as confirmed by the results from BET and XPS measurements [28]. Furthermore, the specific capacitance of the NCF (153.8 F g^{-1}) is higher than previously reported values for N-doped CNT (44.3 F g^{-1}) and N-doped graphene (110 F g^{-1}) [29, 30]. The specific capacitances of 3.5 wt% for both the bare TiO_2 in the CF and the N-doped TiO_2/TiN in the NCF were measured to be 0.04 F g^{-1} and 0.53 F g^{-1} (data not shown), respectively, indicating that the effects of such impurities can be negligible. This result demonstrates a high potential for the application of the NCF to be commercialized. The NCF also showed reproducible and highly stable cycle life during 6000 charge-discharge measurements at a current density of 10 A g^{-1} (figure 7). The slight increment in the specific capacitance with cycling could be due to the release of pore clogging, which results in the increase in the accessible areas for electrolyte ions for charge storage within relatively small pores. It is generally accepted that pore clogging, which can be caused by trapped or blocked electrolyte ions in small pores, may reduce the specific capacitance of the porous electrode material [8, 31, 32].

The diameter of the semi-circle indicates the interfacial charge transfer resistance between the surface of the electrode material and the electrolyte. The value for the NCF (1.4 Ω) was bigger than those for the CF (0.82 Ω) and the AC (0.78 Ω). This is expected, since the charge transfer of the NCF involves surface redox reactions between the electrolyte ion and the large amount of pyridinic nitrogen functional groups, in addition to the pure EDLC [33, 34]. In an alkaline electrolyte, it has been reported that pyridine-type nitrogen plays a significant role for redox reaction [33]. We can also confirm that the CF and NCF electrodes are not involved in Warburg impedance, which is related to mass transfer resistance, such as ion diffusion and transport from the electrolyte to the electrode's surface, based on the fact that there is no line that intersects the real axis near a −45° angle [35, 36]. A slope of a vertical line at a low frequency region for the NCF and the CF was higher than the one for the AC, suggesting that ion diffusion is more rapid. It is attributed to their unique pore structures with the presence of mesopores, which leads electrolyte ions to be accessed easier than the micropores (~1 nm) of the AC [37]. This is in good agreement with the higher rate capability of the NCF compared to that of the AC, which was examined by galvanostatic measurement, as shown in figure 6(d). The magnitudes of the ESR obtained from the intercept (*x*-axis) for the NCF electrode were determined to be 0.27, which is attributed to the IR drop at the beginning of the galvanostatic discharge curve in figure 6(a) [25, 38].

4. Conclusions

In summary, a nitrogen-doped mesopore/micropore hybrid carbon material was synthesized from used cigarette filters by a one-step process. The results of the electrochemical measurement suggest that the porosity characteristics of the NCF and the CF can provide efficient ion transfer. Moreover, it was suggested that the pseudocapacitive interactions between the electrolyte ions and the nitrogen dopants, as the result of nitrogen doping for the NCF, leads to an increase in specific capacitance. We conclude that further exploration of cigarette filters for a supercapacitor electrode is warranted in the field of commercial power-consuming devices with the reduction of the environmental burden.

Acknowledgments

This research was supported by the Global Frontier R&D Program on Center for Multiscale Energy System funded by

the National Research Foundation under the Ministry of Science, ICT & Future Planning, Korea (NRF-2011-0031571).

References

[1] Mastragostino M and Soavi F 2007 *J. Power Sources* **174** 89–93
[2] He Y B, Li G R, Wang Z L, Su C Y and Tong Y X 2011 *Energy Environ. Sci.* **4** 1288–92
[3] Niu Z, Dong H, Zhu B, Li J, Hng H H, Zhou W, Chen X and Xie S 2013 *Adv. Mater.* **25** 1058–64
[4] Hsia B, Kim M S, Vincent M, Carraro C and Maboudian R 2013 *Carbon* **57** 395–400
[5] Zhu M, Weber C J, Yang Y, Konuma M, Starke U, Kern K and Bittner A M 2008 *Carbon* **46** 1829–40
[6] Simon P and Gogotsi Y 2013 *Accounts Chem. Res.* **46** 1094–103
[7] Beidaghi M and Gogotsi Y 2014 *Energy Environ. Sci.* **7** 867–84
[8] Simon P and Gogotsi Y 2008 *Nat. Mater.* **7** 845–54
[9] Liu N, Shen J and Liu D 2013 *Microporous Mesoporous Mat.* **167** 176–81
[10] Wang D W, Li F, Liu M, Lu G Q and Cheng H M 2008 *Angew. Chem. Int. Ed.* **47** 373–6
[11] Fuertes A B, Lota G, Centeno T A and Frackowiak E 2005 *Electrochim. Acta* **50** 2799–805
[12] Paek E, Pak A J, Kweon K E and Hwang G S 2013 *J. Phys. Chem.* C **117** 5610–6
[13] You B, Wang L, Yao L and Yang J 2013 *Chem. Commun.* **49** 5016–8
[14] Polarz S, Smarsly B and Schattka J H 2002 *Chem. Mater.* **7** 2940–5
[15] Lee M, Yun H J, Yu S and Yi J 2014 *Catal. Commun.* **43** 11–5
[16] Lei Z, Shi F and Lu L 2012 *ACS Appl. Mater. Interfaces* **4** 1058–64
[17] Guo C, Li N, Ji L, Li Y, Yang X, Lu Y and Tu Y 2014 *J. Power Sources* **247** 660–7
[18] Buchmeiser M R, Unold J, Schneider K, Anderson E B, Hermanutz F, Frank E, Müller A and Zinn S 2013 *J. Mater. Chem.* A **1** 13154–63
[19] Wang Y, Su F, Wood C D, Lee J Y and Zhao X S 2008 *Ind. Eng. Chem. Res.* **47** 2294–300
[20] Puls J, Wilson S A and Hölter D 2011 *J. Polym. Environ.* **19** 152–65
[21] Ashraf M W 2012 *Sci. World J.* 729430
[22] Luo W, Wang B, Heron C G, Allen M J, Morre J, Maier C S, Stickle W F and Ji X 2014 *Nano Lett.* **14** 2225–9
[23] Kim N D, Kim W, Joo J B, Oh S, Kim P, Kim Y and Yi J 2008 *J. Power Sources* **180** 671–5
[24] Peng F, Cai L, Yu H, Wang H and Yang J 2008 *J. Solid State Chem.* **181** 130–6
[25] Yang S, Wu X, Chen C, Dong H, Hu W and Wang X 2012 *Chem. Commun.* **48** 2773–5
[26] Kim T Y, Lee H W, Stoller M, Dreyer D R, Bielawski C W, Ruoff R S and Suh K S 2011 *ACS Nano* **5** 436–42
[27] Park S, Nam I, Kim G P, Park J, Kim N D, Kim Y and Yi J 2013 *Chem. Commun.* **49** 1554–2013
[28] Jeong H M, Lee J W, Shin W H, Choi Y J, Shin H J, Kang J K and Choi J W 2011 *Nano Lett.* **11** 2472–7
[29] Jiang B, Tian C, Wang L, Sun L, Chen C, Nong X, Qiao Y and Fu H 2012 *Appl. Surf. Sci.* **258** 3438–43
[30] Zhang Y, Liu C, Wen B, Song X and Li T 2011 *Mater. Lett.* **65** 49–52
[31] Puthusseri D, Aravindan V, Madhavi S and Ogale S 2014 *Energy Environ. Sci.* **7** 728–35
[32] Lee J H, Park N, Kim B G, Jung D S, Im K, Hur J and Choi J W 2013 *ACS Nano* **7** 9366–74
[33] Nasini U B, Bairi V G, Ramasahayam S K, Bourdo S E, Viswanathan T and Shaikh A U 2014 *J. Power Sources* **250** 257–65
[34] Andreas H A and Conway B E 2006 *Electrochim. Acta* **51** 6510–20
[35] Miller J R, Outlaw R A and Holloway B C 2010 *Science* **329** 1637–9
[36] Si P, Ding S, Lou X-W and Kim D-H 2011 *RSC Adv.* **1** 1271–8
[37] Wang X *et al* 2013 *Nat. Commun.* **4** 2905
[38] Zhang L *et al* 2013 *Sci. Rep.* **3** 1408